PHYSICAL REVIEW D **86,** 043510 (2012)

Constraining primordial magnetism

J. Richard Shaw[1,2,*] and Antony Lewis[3,†]

[1]*Kavli Institute for Cosmology, Madingley Road, Cambridge, CB3 0HA, United Kingdom*

[2]*Canadian Institute for Theoretical Astrophysics, 60 St George Street, Toronto, M5S 3H8, Canada*

[3]*Astronomy Center, University of Sussex, Brighton, BN1 9QH, United Kingdom*

(Received 5 July 2010; revised manuscript received 9 January 2012; published 7 August 2012)

Primordial magnetic fields could provide an explanation for the galactic magnetic fields observed today; in which case, they may leave interesting signals in the CMB and the small-scale matter power spectrum. We discuss how to approximately calculate the important nonlinear magnetic effects within the guise of linear perturbation theory and calculate the matter and CMB power spectra including the Sunyaev-Zel'dovich contribution. We then use various cosmological data sets to constrain the form of the magnetic field power spectrum. Using solely large-scale CMB data (WMAP7, QUaD, and ACBAR) we find a 95% C.L. on the variance of the magnetic field at 1 Mpc of $B_\lambda < 6.4$ nG. When we include South Pole Telescope data to constrain the Sunyaev-Zel'dovich effect, we find a revised limit of $B_\lambda < 4.1$ nG. The addition of Sloan Digital Sky Survey Lyman-α data lowers this limit even further, roughly constraining the magnetic field to $B_\lambda < 1.3$ nG.

DOI: 10.1103/PhysRevD.86.043510 PACS numbers: 98.80.−k

I. INTRODUCTION

Magnetic fields are observed at the 10^{-6} G level in galaxies and clusters not just in the local Universe but up to a redshift of $z \sim 0.7$–2 [1]. Production of magnetic fields within a formed galaxy is extremely difficult, and the consensus is that they are amplified from pregalactic seed fields [2]. One interesting possibility is that these seed fields were primordial in origin, formed in the very early Universe. These seed fields are thought to have originated either in a phase transition in the early Universe or produced directly during inflation. However, these scenarios have problems, the former struggles to produce any significant magnetic fields with the correlation lengths observed [3,4], while many models of inflationary magnetogenesis must produce fields of limited amplitude in order that backreaction does not halt inflation [5].

The observation of magnetic fields up to a redshift of $z \sim 2$ are particularly interesting as the fields have amplitudes ($B \sim 10\ \mu$G) comparable to those observed locally [6]. This evidence seems to disfavor a large dynamo amplification, requiring a larger seed field to produce today's magnetic fields. In the extreme case of there being no dynamo amplification, adiabatic contraction alone could amplify a pregalactic field of around 1 nG (comoving) to the required level.

A stochastic primordial magnetic field not only modifies the standard evolution of the Universe but sources additional scalar, vector, and tensor modes, giving rise to both new temperature and polarization perturbations in the CMB as well as modifying the standard scenario [7–16]; both these contributions alter the matter distribution in the local Universe [17–22]. Our aim in this paper is to see what limits current data places on the level of magnetic fields in the early Universe, and whether this is compatible with a scenario where galactic magnetic fields are seeded by primordial magnetic fields.

Constraints on the strength of a primordial magnetic field come from many areas. The expansion rate at nucleosynthesis places direct limits on the strength of a magnetic field then of $B \lesssim 1\ \mu$G (comoving) [23,24], though this can be strengthened by looking at the constraint on magnetic sourced gravitational waves [25] (also see Sec. IV D). An indirect constraint suggests that primordial magnetic fields must be limited to $B_\lambda \lesssim 10^{-12}$ G to match Faraday rotation measures in clusters [26,27], though this bound is heavily dependent on the modeling of the magnetohydrodynamics during and after cluster formation. Observations of the CMB provide the strongest direct limits, with previous statistical analyses [28–30], finding field strengths of several nG to be consistent with current CMB data, with comparable bounds also coming from limits on the contribution to σ_8 [19,21]. These analyses only looked at the CMB power spectrum and some progress has been made in improving these limits through higher order moments [31] such as the CMB bispectrum [32,33].

This work will depend heavily on the results of a previous paper [16], and will use the same conventions and notation. Where it is necessary to use perturbation theory we use a gauge invariant notation [34,35] similar to the conformal Newtonian gauge. In this work we limit ourselves to a flat ΛCDM universe.

II. NONLINEAR FIELD EVOLUTION

We will consider a stochastic magnetic field $B^i(x^j, \tau)$ generated by some mechanism in the very early Universe.

*jrs65@cita.utoronto.ca
†http://cosmologist.info

As for all the periods of interest the Universe contains a highly ionized plasma; we can use the MHD equations to describe the behavior of the magnetic field. At linear order in the magnetic field

$$\frac{\partial}{\partial\tau}[a^2 B^i(\mathbf{x},\tau)] = 0, \tag{1}$$

and this motivates the definition of a comoving magnetic field, $\hat{B}^i(\mathbf{x},\tau) = a^2 B^i(\mathbf{x},\tau)$ which is time independent at linear order. Using this we can write the nonzero components of the magnetic energy-momentum tensor as

$$T_0^0 = -\frac{1}{8\pi a^4}\hat{B}^2(\mathbf{x}), \tag{2a}$$

$$T_j^i = \frac{1}{4\pi a^4}\left(\frac{1}{2}\hat{B}^2(\mathbf{x})\delta_j^i - \hat{B}^i(\mathbf{x})\hat{B}_j(\mathbf{x})\right). \tag{2b}$$

As there is no magnetic field on the background, the perturbations of the stochastic background are manifestly gauge invariant. We construct density and anisotropic stress perturbations, Δ_B and Π_B, defined by

$$T_0^0 = -\rho_\gamma \Delta_B, \tag{3a}$$

$$T_j^i = p_\gamma(\Delta_B \delta_j^i + \Pi_B{}^i{}_j), \tag{3b}$$

where we include the factors of ρ_γ and p_γ to take account of the a^{-4} factors. As usual the anisotropic stress $\Pi_B{}^i{}_j$ can be decomposed into scalar, vector, and tensor contributions.

At higher order the comoving magnetic field obeys

$$\begin{aligned}\partial_\tau \hat{B}^i &= [\nabla\times(\mathbf{v}\times\hat{\mathbf{B}}) + \eta\nabla^2\hat{\mathbf{B}}]^i \\ &= \epsilon^{ijk}\epsilon_{klm}\partial_j(v^l\hat{B}^m) + \eta\partial_j\partial^j\hat{B}^i,\end{aligned} \tag{4}$$

where $\mathbf{v}$ is the baryon velocity and η is the magnetic diffusivity. In a highly conductive medium η is negligible and so we will set it to zero from here onward. As (4) is nonlinear the magnetic field evolution cannot be treated accurately in the standard linearized Einstein-Boltzmann approach. The standard approach is to separate the higher order evolution of the magnetic field into two effects that are physically well-motivated, a damping due to the radiation viscosity and the effect of the magnetic Jeans length (for extended discussions, see [36–39]). We follow the same route in this work, modifying the linear evolution equations to capture the essential physics without resorting to a higher order calculation. Though a more detailed second order calculation would be desirable, it would be computationally unfeasible to use this in a Markov-chain Monte Carlo analysis of cosmological data.

The first nonlinear contribution we address is the magnetic counterpart of the Jeans effect. As gravitational collapse causes baryon density perturbations to grow the pressure in the gas is increased and eventually halts the growth. When present, a magnetic field gives an additional contribution to the pressure. As a baryon overdensity collapses it compresses the large-scale field, generating an increase in the magnetic pressure at the scale of the baryon perturbation. In a magnetized medium there are multiple modes that could be excited, but we expect the Jeans effect to be mediated primarily by the fastest (the fast magnetosonic mode), which corresponds to the normal acoustic mode in the limit of a small magnetic field [40]. The simplest way of encapsulating this is to consider it as a modification of the baryon sound speed, to the speed of the fast magneto-acoustic mode [38,40], $c_s^2 \to c_{s,b}^2 + \alpha v_A^2$ where α is an angular factor depending on the exact velocity and field orientation. To include this in our work we modify the evolution of the baryon velocity to

$$\begin{aligned}\dot{\theta}_b = &-\mathcal{H}\theta_b + k^2\Psi + R\tau_c^{-1}(\theta_\gamma - \theta_b) \\ &+\frac{1}{2}k^2 R\left(\frac{1}{2}\Delta_{B,0} - \frac{1}{3}\Pi_{B,0}^{(0)}\right) + k^2\left(c_{s,b}^2 + \frac{2}{9}v_A^2\right)\Delta_b,\end{aligned} \tag{5}$$

where $c_{s,b}$ remains the standard unmagnetized baryon sound speed, and we have defined the Alfvén velocity v_A as

$$v_A^2 = \frac{1}{4\pi\rho a^4}\langle\hat{B}^2\rangle_k \tag{6}$$

where ρ is the density of the conducting fluid, and $\langle\hat{B}^2\rangle_k$ is the variance of the field from scales larger than k. We discuss this effect in more detail in Appendix A, motivating the specific form of the modification in (5), in particular the factor $2/9$ multiplying the Alfvén velocity. It is important to note that as this effect is nonlinear, the modes do not decouple and even when evolving the standard adiabatic mode we must add in the Alfvén velocity term.

Radiation free-streaming is particularly important for magnetic fields and is the most important source of damping on large scales [37]. Prior to free-streaming, there are many photon-baryon scatterings per wavelength, and the radiation and baryons appear like a single tightly-coupled conducting fluid. However, when the photons start to free-stream they decouple from the baryon fluid and this becomes the sole conducting fluid. While the baryons are no longer tightly-coupled to the photons, there is still enough scattering to exert a significant drag force on the fluid, and this causes damping on propagating magnetic waves.

When the photons decouple from a particular scale, the fluid no longer feels the radiation pressure, and the magnetic pressure dominates the baryon pressure for $B \gtrsim 0.1$ nG. In this regime, in addition to Alfvén modes, magneto-acoustic modes are also significant.

Properly accounting for the damping in the radiation free-streaming regime requires the use of the full Boltzmann system for the photons, a procedure that is complicated by the necessity of including nonlinear magnetic effects. Instead we use the prescription of [36], who analyzed the evolution of Alfvén modes in the presence of a homogeneous radiation drag force. They find that the magnetic field on small scales damped approximately as

$$\hat{B}^i(\mathbf{k}) = \hat{B}_0^i(\mathbf{k})\exp\left(-k^2\int^{\tau_*} v_A^2\tau_c d\tau\right), \tag{7}$$

where v_A and τ_c are defined above, and τ_* is the time of last scattering. For magneto-acoustic modes, the damping is similar to that of (7) with the Alfvén velocity v_A replaced with the baryon sound speed $c_{s,b}$, causing them to damp on smaller scales [36,37]. For simplicity, we will treat the field as damping solely on the largest scale, that of the Alfvén modes.

To account for this damping in our work, we allow the linear perturbations Δ_B and Π_B to evolve. This is in contrast to other work in the literature [13,14,28] where the perturbations are constant for all time and the damping is imposed as a cutoff on the initial power spectrum. This is implemented by constructing effective differential equations for the two perturbations for $\tau < \tau_*$

$$\dot{\Delta}_B = -2k^2 v_A^2 \tau_c \Delta_B, \qquad \dot{\Pi}_B = -2k^2 v_A^2 \tau_c \Pi_B. \tag{8}$$

For $\tau > \tau_*$, we set $\dot{\Delta}_B$ and $\dot{\Pi}_B$ to zero, as after recombination there is less than one scattering per Hubble time and the damping is negligible. To ensure that energy conservation is maintained we presume that this is transferred equally into the photon-baryon fluid. We modify the baryon density equation to

$$\dot{\Delta}_b = -\theta_b + 3\dot{\Phi} + \frac{2k^2}{1+R^{-1}} v_A^2 \tau_c \Delta_B, \tag{9}$$

and the photon density equation to

$$\dot{\Delta}_\gamma = -\frac{4}{3}\theta_\gamma + 4\dot{\Phi} + \frac{2k^2}{1+R^{-1}} v_A^2 \tau_c \Delta_B, \tag{10}$$

where we have added the final term in both of the above equations. Practically, ensuring energy conservation makes little difference to the results.

There is further avenue of decay for the magnetic fields, through the damping of MHD turbulence in the post-recombination Universe [41]. This effect is able to damp scales larger than those affected by free-streaming but smaller than the Jeans length, though its magnitude is uncertain. This extra damping is not included in this work, however, as this only modifies modes smaller than the Jeans length we do not expect it to change our constraints (which are based on data probing larger scales).

One might worry that the modification to the evolution equations above invalidate the initial conditions for the magnetic modes that we are using [16], which were derived for the unmodified equations. First, the modification to (5) takes the form of a modification to the baryon sound speed, as this is higher order in the initial conditions we do not expect it to affect our results. The further changes made are to (8)–(10), and are all proportional to $k^2\tau\tau_c$ which is negligible on superhorizon scales during radiation domination.

III. MAGNETIC MATTER POWER SPECTRUM

Using the above modifications to the evolution equations we are able to calculate matter power spectra including approximate treatments of the important nonlinear effects. The remaining input is the statistics of the initial magnetic perturbations Δ_B and Π_B. We assume that at some early time the comoving magnetic field power spectrum is described by a power spectrum

$$\langle \hat{B}_i(\mathbf{k})\hat{B}_j^*(\mathbf{k}')\rangle = (2\pi)^3\delta(\mathbf{k}-\mathbf{k}')\frac{P_{ij}(\hat{k})}{2}P_B(k), \tag{11}$$

where $P_{ij} = \delta_{ij} - \hat{k}_i\hat{k}_j$, and we will not consider helicity. The magnetic field power spectrum is

$$P_B(k) = Ak^{n_B}. \tag{12}$$

We will use the spectral index n_B as defined, but it is conventional to give the amplitude of the spectrum in terms of the variance B_λ^2 of the magnetic field strength at a scale λ (we choose $\lambda = 1$ Mpc to agree with the bulk of the literature). This gives

$$A = \frac{(2\pi)^{n_B+5}B_\lambda^2}{2\Gamma(\frac{n_B+3}{2})k_\lambda^{n_B+3}}. \tag{13}$$

To calculate the two required power spectra $P_{\Delta_B}(k)$, $P_{\Pi_B}(k)$ and the cross spectrum $P_{\Delta_B\Pi_B}(k)$ requires convolutions of the magnetic power spectrum. We use the results of a previous paper [16], which allows us to reduce the convolution into a dimensionless integral depending only on n_B. We numerically evaluate these at a large number of values such that we can accurately interpolate to find power spectra at an arbitrary n_B. It is important to note that as we are including the damping and Jeans effects in the evolution of the magnetic perturbations we can safely avoid imposing a cutoff in the initial power spectrum as used in other work [13,30].

In Fig. 1 we show the consequence of the two nonlinear effects on the matter power spectrum. The first thing to note is that the linear theory magnetic power spectrum grows as $P(k) \propto k$. On subhorizon scales during matter domination, we can combine the evolution equations for baryons and dark matter to give an equation for the total matter perturbation $\Delta_m = R_b\Delta_b + R_c\Delta_c$

$$\ddot{\Delta}_m + \mathcal{H}\dot{\Delta}_m - \frac{3}{2}\mathcal{H}^2\Delta_m = \frac{\rho_\gamma}{\rho_m}k^2 L_B, \tag{14}$$

where the Lorentz force $L_B = \frac{2}{3}(\frac{1}{3}\Pi_B - \Delta_B)$, and we neglect pressure terms in $c_{s,b}^2$. In these limits the equation has a simple solution for the magnetic mode

$$\Delta_m = R_b L_B \frac{\rho_\gamma(\tau_i)}{\rho_b(\tau_i)}(k\tau_i)^2\left[\frac{1}{10}\left(\frac{\tau}{\tau_i}\right)^2 + \ldots\right], \tag{15}$$

where we have included only the leading order term, and τ_i is the time when the mode starts to grow significantly. This is the time that the baryon perturbation decouples from the photons. Provided this time is similar across a range of scales (correct for larger scales), we can expect $P_m(k) \propto k^4 P_{L_B}(k)$; for nearly scale invariant magnetic field spectra this gives $P_m(k) \propto k$.

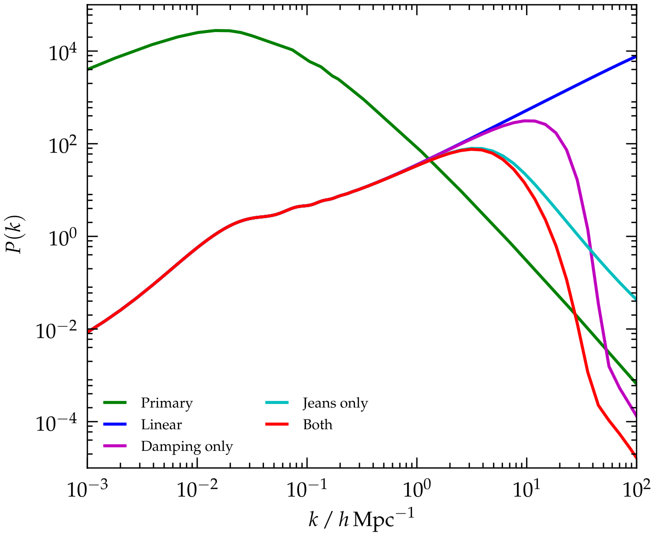

FIG. 1 (color online). The additional nonlinear effects modify the magnetic power spectrum. We plot the linear-only behavior, the diffusion damping of the magnetic field, the magnetic pressure support, and both effects combined. For comparison we also include the primary adiabatic mode. All these plots are calculated with a magnetic field strength of $B_\lambda = 5$ nG and spectral index $n_B = -2.9$.

The effect of including the magnetic pressure increases the Jeans length, and thus causes smaller scales to oscillate. In matter domination, the comoving magnetic Jeans wave number is constant and thus larger k grow very little after recombination. On even larger scales the diffusion damping of the magnetic fields causes the source for the later growth

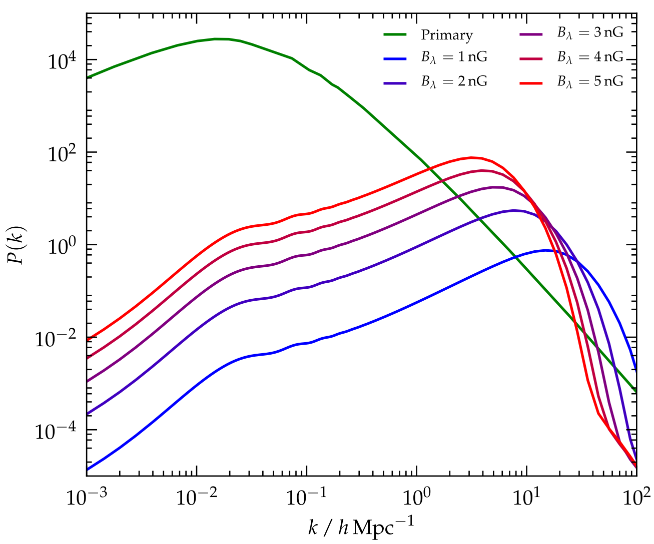

FIG. 2 (color online). The full matter power spectrum with all nonlinear effects at a variety of magnetic field strengths between $B_\lambda = 1$–5 nG. We have held the magnetic spectral index constant at $n_B = -2.9$. The power spectrum amplitude increases strongly with that of the magnetic field, however the two scales associated with the diffusion damping and magnetic Jeans length also increase rapidly.

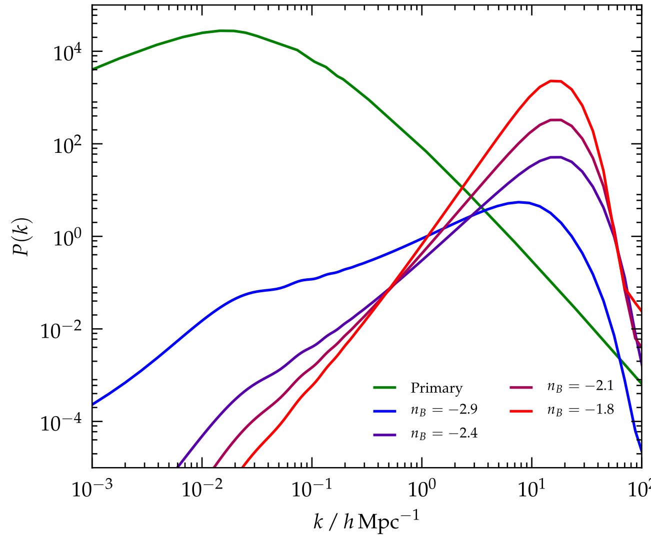

FIG. 3 (color online). The full matter power spectrum with all nonlinear effects at a variety of magnetic spectral indices between $n_B = -2.9$ to -1.8. The amplitude is fixed at $B_\lambda = 2$ nG.

of the magnetic fields to be exponentially suppressed. This leads to much slower growth in the matter perturbations, and an effective cutoff beyond which there are no significant perturbations sourced. The scales at which these effects start roughly agree with the estimates of [20,36,38], where both are expected to scale like $k_c \propto B_\lambda^{-(n+5)/2}$.

In Figs. 2 and 3, we plot the effect on the matter power spectrum of the amplitude and tilt of the magnetic spectrum. Figure 2 shows that the relative contrast between the peak magnetic and primary contributions stay roughly constant as the amplitude B_λ is varied. This occurs as a consequence of the fact that the matter power spectrum at the damping cutoff is $\propto B_\lambda^4 k_c$, while the primary spectrum $\propto k_c^{-3}$. However as the damping wave number $k_c \propto B_\lambda^{-1}$ for nearly scale invariant spectra, the ratio between the two is constant.

Both the magnetic damping and Jeans effects give small changes to the CMB power spectra at very high l. The maximum scale that is affected by the magnetic damping is around $k_D \sim 1h$ Mpc^{-1} and this changes the CMB power spectra on scales $l > D_A k_D \sim 10^4$. For $l < 10^4$ the power spectra are essentially the same as those shown in [16], though in this work our power spectra are evolved from the modified equations.

IV. RESULTS

We have used versions of CAMB [42] and COSMOMC [43] modified to generate the magnetic contributions to both the CMB angular power spectrum and the matter power spectrum.[1] We limit ourselves to the most important magnetic

[1]The modified version of CAMB and the adaptation of COSMOMC to use will be available from http://camb.info/jrs.

contributions in this work, the magnetic scalar and vector modes and the tensor passive mode. We sample with a flat prior in the standard set of cosmological parameters $\{\Omega_b h^2, \Omega_c h^2, \theta, \tau, n_s, \log(10^{10}A_s)\}$, assuming a flat ΛCDM universe. To describe the magnetic fields we supplement this with three parameters, the magnetic power spectrum amplitude B_λ, and spectral index n_B. We also need to specify the production time of the magnetic fields τ_B to calculate the passive modes. The tensor passive mode that we calculate has the same structure as the standard tensor mode with amplitude

$$H^{(2)} = R_\gamma \Pi_B^{(2)}\left[\log(\tau_\nu/\tau_B) + \frac{5}{8R_\gamma} - 1\right], \qquad (16)$$

where τ_ν is the time of neutrino decoupling (see [16]). Rather than directly specifying the magnetic field production time we use a proxy $r_B = \log_{10}(\tau_\nu/\tau_B)$, such that $H^{(2)} \sim \log(10) R_\gamma \Pi_B^{(2)} r_B$.

For priors on the magnetic quantities we choose a flat prior in $B_\lambda < 10$ nG. For r_B we use a flat prior with bounds $6 \le r_B \le 17$ corresponding to magnetic field production between the electroweak phase transition and reheating at the GUT scale. Finally for the spectral index we use a flat prior $-2.95 \le n_B \le -1.6$, the lower bound of this comes from the fact that there is an infrared divergence for $n_B \le -3$. The upper bound is from the fact that we are primarily interested in primordial fields produced in the early Universe (prior to nucleosynthesis); the work of [25] suggests that larger spectral indices are ruled out by nucleosynthesis constraints (see Sec. IV D). Other than the upper bound on the spectral index, our results should be valid for fields produced at later epochs.

A. CMB-only

Primordial magnetic fields contribute both passive and compensated scalar and tensor modes, as well as a compensated vector mode. However, the significant contributions are from the passive tensor mode, and the compensated vector mode, which are important on large and small scales, respectively [16]. For comparison to CMB data (for scales $l \lesssim 3000$) we need only need calculate these two.

We use the recent WMAP 7 yr release [44] along with the final data from QUaD [45] and ACBAR [46] for $l < 3000$. We also use the Hubble Key Project data [47], BBN data, Union Supernova dataset [48], and BAO data from SDSS DR7 [49]. To account for the Sunyaev–Zel'dovich effect at high multipoles we adopt the standard treatment and use the WMAP template [44]. This requires an extra parameter for its normalization A_{SZ} which we treat as a nuisance parameter and marginalize over.

The resulting constraints are shown in Fig. 4, which are in broad agreement with those of Ref. [30]. We have included only the magnetic amplitude B_λ and spectral index n_B, marginalizing over the other parameters. The

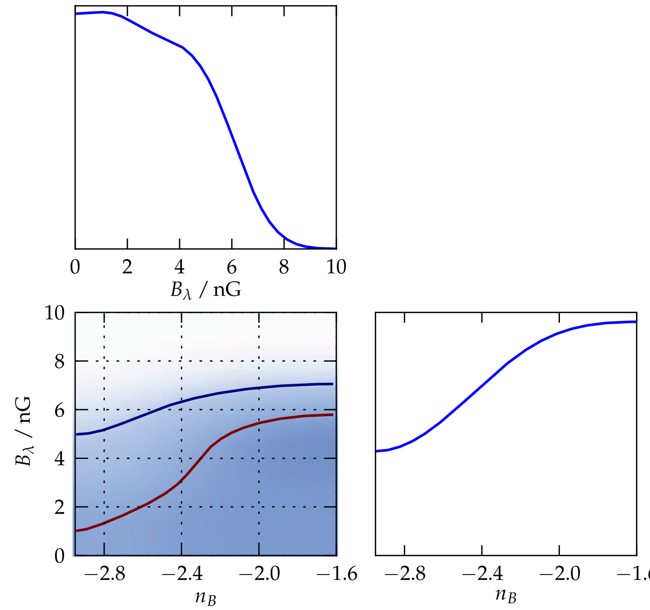

FIG. 4 (color online). The CMB-only (WMAP7 + QUAD + ACBAR) constraints on the magnetic field amplitude and spectral index. The top left plot is the marginalized constraint solely on the magnetic field, and the bottom right is the marginal constraint on its spectral index. The bottom left plot is the joint constraint (marginalized over the other cosmological parameters), with contours for one and two sigma errors.

standard cosmological parameters are not shown as they are in agreement with their values in a universe with no primordial magnetic fields. We have also chosen not to include r_B as it is unconstrained by the data (see Fig. 5). This is a manifestation of the fact that the tensor passive mode can be only significant at large magnetic amplitudes, and these are already excluded by the magnetic vector mode. From this we calculate a 95% C.L. of $B_\lambda < 6.4$ nG.

The constraints on the magnetic parameter space are unchanged when adding in large-scale matter power data sets such as 2dF [50] and SDSS LRG data from DR4 [51],[2] though the cosmological parameters change as expected. The reason can be seen from Fig. 2, as the magnetic contributions are only significant for $k \gtrsim 1h$ Mpc^{-1}, and the galaxy redshift surveys probe only up to $k \sim 0.2h$ Mpc^{-1}. We will include this data for the remainder of this paper.

B. Sunyaev—Zel'dovich effect

Recent work [20] has suggested that the Sunyaev–Zel'dovich (SZ) effect may be able to give tight constraints on the magnetic power spectrum. As the magnetic fields cause an increase in the small-scale matter power

[2]We do not use the latest SDSS DR7 data [52] due to complications modifying its likelihood calculation to include the magnetic field matter power spectrum.

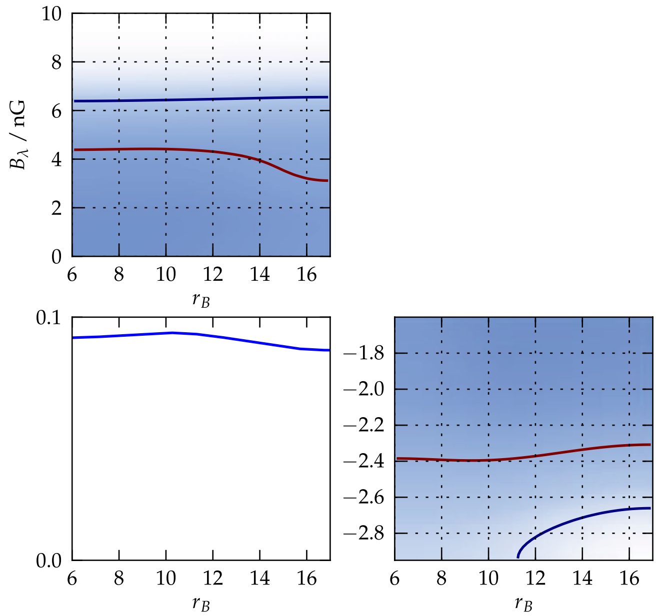

FIG. 5 (color online). The CMB-only marginal constraint on the production time ratio $r_B = \log_{10}(\tau_\nu/\tau_B)$ (bottom left), along with the correlations with the magnetic field amplitude (top left) and spectral index (bottom right). Even in the CMB-only constraint r_B is largely unconstrained and has minimal correlation with the other parameters, being only important in the case of very large magnetic fields, and a very red spectral index.

spectrum, this gives rise to a large number of small mass halos and thus a rise in the SZ angular power spectrum. The recent release of data from the South Pole Telescope (SPT) [53] provides CMB observations up to $l \sim 10^4$ that we will compare to.

We follow the general method of [20], using the prescription of [54] to calculate the thermal SZ angular power spectrum from the matter power spectrum, which we have calculated using our modified version of CAMB. We give the details of this calculation in Appendix B. In addition to the SZ contribution the magnetic vector mode gives a significant addition to the small-scale CMB power, which must be included. We do not include the kinetic SZ spectrum which is subdominant to the thermal spectrum. We also note that the non-Gaussian statistics of the SZ effect can significantly increase its intrinsic variance [55]; we do not account for this within this paper.

As well as the data sets for the CMB-only constraints, and the SPT data, we have also included the large-scale matter power data. When generating the SZ power spectrum we must include all contributions, both the adiabatic and magnetic contributions, as such we do not add in an SZ template, and thus A_{SZ} is no longer sampled over. The SPT data contains a further small-scale contribution from the unresolved point sources, both from star-forming and radio galaxies (see Fig. 6). The exact value must be fit from the bandpowers (in the analysis of [53] it is poorly constrained with $C_l^{\rm ps} = (6.2 \pm 6.4) \times 10^{-7}\ \mu{\rm K}^2$). We expect that

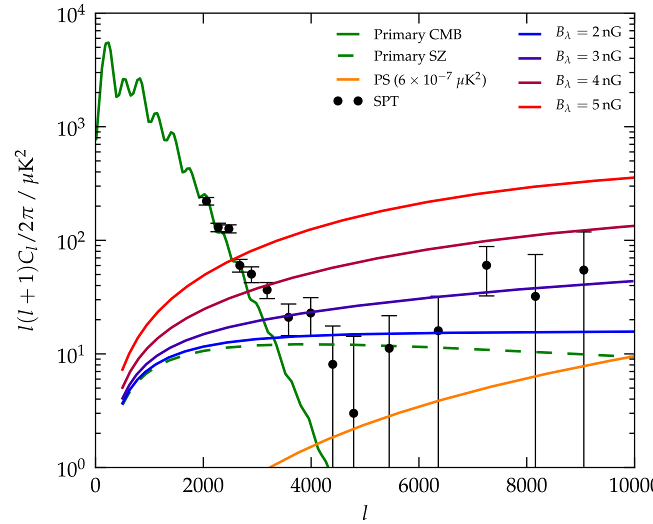

FIG. 6 (color online). The angular power spectrum of the CMB and the SZ contributions to it. We plot the SZ contribution from the primary adiabatic mode only, and in combination with four magnetic field strengths $B_\lambda = 2$–5 nG, with a magnetic spectral index of $n_B = -2.4$. We also plot the band powers from SPT, and the estimate of the residual point source contribution (labeled PS). Both the SZ contribution and the SPT data are at 150 GHz.

neglecting this contribution will result in a small increase to our upper limits.

The magnetic contribution to the SZ power spectrum from our calculations is smaller than that of [20]. Differences between our calculations, such as in finding the amplitude of the matter perturbations and treating the nonlinear effects, make it difficult to give a single reason for this.

Figure 7 shows the marginalized probability distributions for the magnetic parameters (again we do not plot r_B). The addition of the SPT data has excluded much of the parameter space that was allowed when including primary CMB effects only, especially the region with large magnetic field and blue spectral index, which gives the most dramatic change in the matter power spectrum (see Fig. 3). This gives a large decrease in the 95% C.L. of the magnetic amplitude to $B_\lambda < 4.1$ nG.

C. Lyman alpha data

It is clear from both Figs. 2 and 3 that the small-scale matter power spectrum is significantly affected by the presence of a primordial magnetic field. Unfortunately galaxy redshift surveys such as SDSS probe only as far as $k \lesssim 0.2h$ Mpc^{-1}, scales too large to be affected by the magnetic fields. However, observations of the Lyman-α flux power spectrum probe the matter density power spectrum to scales as small as $k \sim 5h$ Mpc^{-1} and may be able to give a much more powerful constraint. Unfortunately there is no simple analytic mapping from the observations to the matter spectrum, so cosmological constraints need to

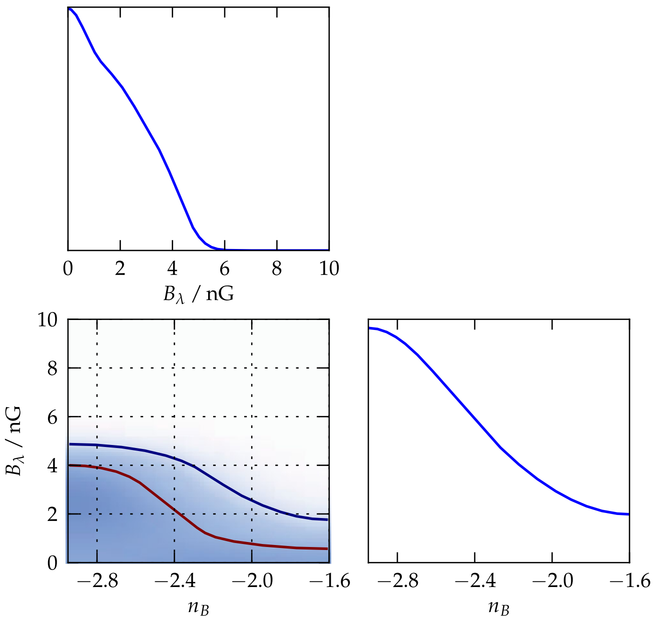

FIG. 7 (color online). The CMB and SZ constraints on the magnetic field amplitude and spectral index. The individual plots are equivalent to those in Fig. 4. Calculating the magnetic SZ contributions with the addition of SPT data has restricted the parameter space to lower amplitudes and redder spectral indices than the large-scale CMB data.

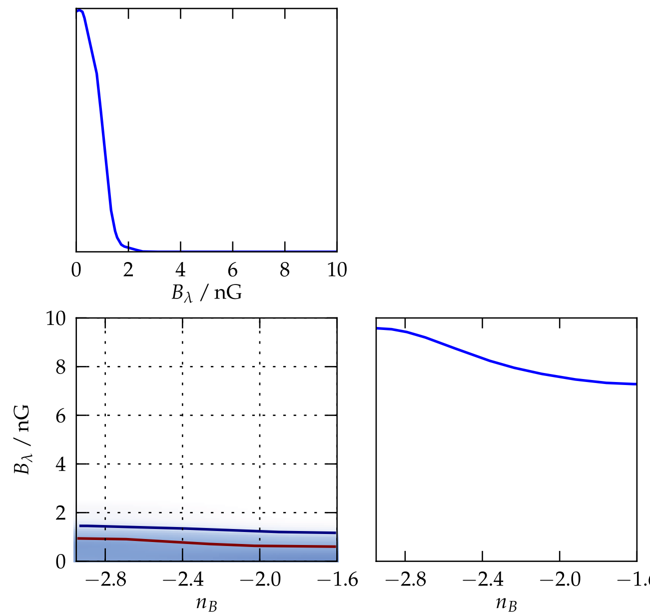

FIG. 8 (color online). Constraints on the magnetic field amplitude and spectral index using CMB and matter power data, including Lyman-α data. The Lyman-α data, which probes the small-scale matter distribution, has dramatically reduced the allowable parameter space, to a range of small amplitudes ($B_\lambda \lesssim 1.5$ nG) roughly independent of spectral index n_B.

be obtained by comparison to simulations [56]. A fully consistent analysis including magnetic fields is beyond the scope of this paper; instead we use a very rough simple approximation to the likelihood.

We use the standard Lyman-α module in COSMOMC which is based on the work of [56]. This finds an effective amplitude and spectral index about a pivot scale of $k = 0.009\ \mathrm{s\,km}^{-1}$ (roughly $k \sim 1h\ \mathrm{Mpc}^{-1}$). It calculates a likelihood from these by interpolating between a set of simulations compared to SDSS quasar data. Because of the large difference between our power spectra (when including magnetic effects) and those of ΛCDM we cannot expect the likelihoods to be very accurate, especially at large magnetic amplitudes and blue spectral indices, where the effect is greatest. However for the pivot scale, and range of scales probed by the SDSS spectra used $k \lesssim 0.02\ \mathrm{s\,km}^{-1}$, the magnetic contribution is generally small compared to that of the primary adiabatic mode. In this light our results should be viewed as an approximation to the constraints that a more sophisticated likelihood approach would achieve.

The magnetic parameter space is significantly constricted by the use of the Lyman-α data (see Fig. 8) with the allowed region for B_λ being largely independent of the spectral index n_B. As the Lyman-α pivot scale ($k \sim 1h\ \mathrm{Mpc}^{-1}$) coincides with the scale at which the magnetic matter power spectrum amplitudes are very similar across a large range of n_B. This is to be expected as the Lyman-α pivot ($k \sim 1h^{-1}\mathrm{Mpc}^{-1}$) coincides with the scale at which the magnetic matter power spectrum amplitude is similar across a broad range of n_B. Overall this results in a 95% C.L. of $B_\lambda < 1.3$ nG.

D. Nucleosynthesis constraints

Nucleosynthesis places strong constraints on the amount of energy density in gravitational waves allowed in the Universe, giving a limit of $\Omega_{\mathrm{GW}} \lesssim 1.1 \times 10^{-6}$ [57]. Prior to neutrino decoupling the anisotropic stress of an inhomogeneous magnetic field on superhorizon scales sources gravitational waves,[3] this allows the small-scale magnetic fields to transfer some of their energy into gravitational waves before it is dissipated into the photon- baryon plasma [25]. This process is quite efficient, and gives the gravitational waves a significant fraction of the original magnetic energy (see [58] for an intuitive explanation of this). As the magnetic field energy density is necessarily blue, there is more energy density in the smallest scale fluctuations. This allows us to strengthen the usual constraints on the total magnetic energy density which only take into account the energy remaining in the field at nucleosynthesis by constraining Ω_{GW} which is sourced at a time when much smaller scales have not been damped. We take Eq. (33) from [25] adapted to our conventions, yielding

[3]These are the same as tensor passive modes [16], though they stop growing when they enter the horizon prior to neutrino decoupling.

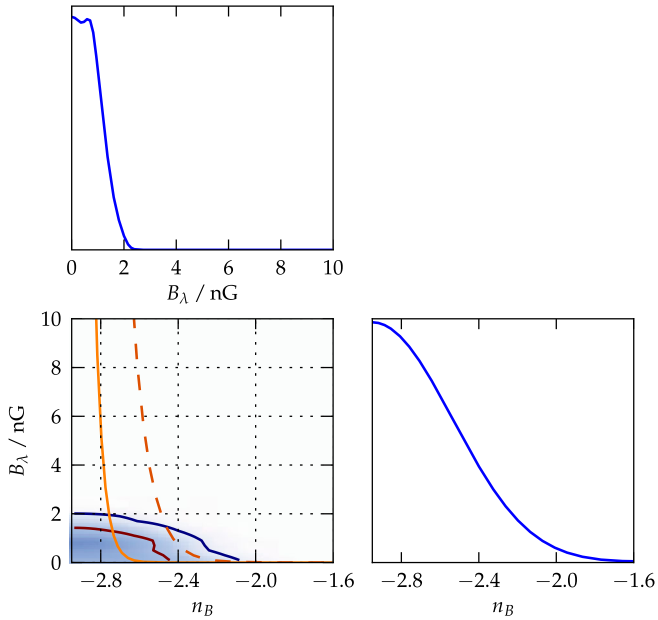

FIG. 9 (color online). Constraints on the magnetic parameter space from Lyman-α data including the nucleosynthesis constraints of [25]. The solid- and dashed-orange lines give the upper bounds in amplitude of a magnetic field produced at GUT scale inflation and the electroweak phase transition, respectively. This corresponds to our priors.

$$B_\lambda/\mathrm{nG} < 700h\left[2^{((n+5)/2)}\Gamma\left(\frac{n+5}{2}\right)\right]^{1/2} 10^{-((n+3)/2)(4+r_B)}. \tag{17}$$

It is essential to note that this assumes that the magnetic field is well-described by a single power law across a vast range of scales—from the pivot scale at $k = 1\ \mathrm{Mpc}^{-1}$ up to at least $k = 10^{10}\ \mathrm{Mpc}^{-1}$, the horizon scale at the electroweak phase transition. Depending on how the magnetic field is generated this assumption may break down—any freedom to reduce small scale power would significantly weaken the constraints.

In Fig. 9 we show the probability distribution of the magnetic parameters when combining the nucleosynthesis constraint with the Lyman-α data of Sec. IV C. As we would expect this reduces the allowed parameter spaces to redder spectral indices $n_B \lesssim -2$. Because of this the limits on the amplitude are slightly enlarged with the 95% C.L. becoming $B_\lambda < 1.6$ nG.

V. CONCLUSION

As we have seen in this paper, when considering the magnetic contributions to the matter power spectrum it is essential to treat important small-scale, nonlinear effects. We have demonstrated a technique for approximating the main nonlinear effects within linear perturbation theory, and have incorporated this into a modified version of CAMB. This gives an alternative to the common approach of incorporating these effects directly into the initial power spectrum, such as in Ref. [30].

We have used our theoretical predictions to place constraints on the allowable magnetic field amplitude given various data sets. Where all limits are at 95% confidence, using CMB data only we find $B_\lambda < 6.4$ nG, with a redder spectral index favored. As the presence of a stochastic magnetic field gives significant modifications to the small-scale matter distribution, we also look at the constraints when adding two probes of it: the Sunyaev–Zel'dovich effect measured by SPT [53], which gives a limit of $B_\lambda < 4.1$ nG, and Lyman-α forest data from SDSS [56], which gives a rough constraint of $B_\lambda \lesssim 1.3$ nG.

While the addition of the small-scale matter data gives a large reduction in the allowed amplitude of a primordial magnetic field (certainly when using Lyman-α data), this is still roughly consistent with a scenario where current galactic fields are formed solely by adiabatic contraction of primordial fields. Increasing the accuracy of measurements at the scales we can currently probe with data will provide limited gains: since the magnetic power spectrum increases with B_λ^4, significantly decreasing the errors on matter power spectrum measurements will produce less impressive gains in the upper limit on B_λ. However, if better observations and modeling allow accurate comparison to smaller scales there should be an almost linear decrease in the upper limit with the smallest scale probed. This would seem to provide the best opportunity for testing the primordial field hypothesis.

ACKNOWLEDGMENTS

We would like to thank Steven Gratton, Simeon Bird, Chiara Caprini, and Camille Bonvin for useful discussions. J. R. S. was supported by Science Technologies Facilities Council (STFC). A. L. acknowledges support from PPARC/STFC .

APPENDIX A: MOTIVATING THE MAGNETIC JEANS EFFECT

To analyze the magnetic Jeans effect we need to look at the nonlinear evolution of the field perturbations. First let us construct Δ^{ij}, a quadratic combination of the magnetic field

$$\Delta^{ij} = \frac{1}{4\pi\rho_\gamma a^4}\hat{B}^i\hat{B}^j, \tag{A1}$$

with the normalization chosen such that it is conveniently close to the magnetic perturbations

$$\Delta_B = \frac{1}{2}\Delta^k_k, \qquad \Pi^{ij}_B = \Delta^k_k\delta^{ij} - 3\Delta^{ij}. \tag{A2}$$

We are interested in the time evolution of Δ^{ij}, and thus want to calculate the derivative $\dot{\Delta}^{ij} = \frac{1}{2\pi\rho_\gamma a^4}\hat{B}^{(i}\partial_\tau\hat{B}^{j)}$, where the parentheses indicate symmetrization with respect to the enclosed indices. It will be useful to reexpress (4) by expanding the Levi-Civita symbols

$$\partial_\tau \hat{B}^i = \hat{B}^k(\partial_k v^i) - v^k(\partial_k \hat{B}^i) - \hat{B}^i \partial_k v^k. \tag{A3}$$

Using (A3) we can calculate the time derivative of $\dot{\Delta}^{ij}$

$$\dot{\Delta}^{ij} = 2(\partial_k v^{(i)})\Delta^{j)k} - 2(\partial_k v^k)\Delta^{ij} - v^k(\partial_k \Delta^{ij}). \tag{A4}$$

Using the definitions of (A2) we can split the above into equations for each of the perturbations Δ_B and Π_B. First

$$\dot{\Delta}_B = -\frac{4}{3}\Delta_B\theta_b - v^k(\partial_k\Delta_B) - \frac{1}{3}\sigma_{kl}\Pi_B^{kl}, \tag{A5}$$

where we have only included terms up to second order, and we have decomposed

$$\partial_i v_j = \frac{1}{3}\theta_b\delta_{ij} + \sigma_{ij} + \omega_{ij} \tag{A6}$$

at linear order. Physically θ_b is the divergence of the baryon 3-velocity, and σ_{ij} is its shear; we will neglect the antisymmetric vorticity tensor ω_{ij}. Second, the magnetic

anisotropic stress evolves as

$$\dot{\Pi}_B^{ij} = -\frac{4}{3}\theta_b\Pi_B^{ij} - v^k\partial_k\Pi_B^{ij} - 4\sigma^{ij}\Delta_B + 2\sigma_k{}^{(i}\Pi_B^{j)k} - \frac{2}{3}\sigma_{kl}\Pi_B^{kl}\delta^{ij}. \tag{A7}$$

In this paper we do not attempt a fully self-consistent nonlinear analysis. Instead, we try to identify the most important nonlinear effects and then model them using an approximate method that is at least as consistent as most previous work. Here we are interested in the magnetic Jeans instability—the isotropic part of this effect is described by the first terms on the right-hand side of (A5) and (A7),

$$\dot{\Delta}_B = -\frac{4}{3}\Delta_B\theta_b, \qquad \dot{\Pi}_B^{ij} = -\frac{4}{3}\Pi_B^{ij}\theta_b, \tag{A8}$$

corresponding to an enhancement $\propto (\rho_b/\rho_b^0)^{4/3}$ as a perturbation collapses to density ρ_b compared to a background value of ρ_b^0. To leading order we can use the linear baryon density evolution equation

$$\dot{\Delta}_b = -\theta_b + 3\dot{\Phi} \tag{A9}$$

to replace θ_b, and neglect $\dot{\Phi}$ on the small scales of interest, giving

$$\Delta_B = \Delta_{B,0}\left(1 + \frac{4}{3}\Delta_b\right) \qquad \Pi_B^{ij} = \Pi_{B,0}^{ij}\left(1 + \frac{4}{3}\Delta_b\right), \tag{A10}$$

where $\Delta_{B,0}$ and $\Pi_{B,0}$ are the magnetic perturbations at some initial time where the baryon perturbation Δ_b was much smaller than its present value. The linearized equation for the evolution of the baryon velocities in Fourier space is

$$\dot{\theta}_b = -\mathcal{H}\theta_b + k^2c_{s,b}^2\Delta_b + k^2\Psi + R\tau_c^{-1}(\theta_\gamma - \theta_b) + \frac{1}{2}k^2R\left(\frac{1}{2}\Delta_B - \frac{1}{3}\Pi_B^{(0)}\right), \tag{A11}$$

where τ_c is defined as $\tau_c = 1/(an_e\sigma_T)$, $c_{s,b}$ the baryon sound speed, $R = 4\rho_\gamma/3\rho_b$, and the last term is the magnetic interaction, the Lorentz force. To include the magnetic field evolution in this, we use Eq. (A10), and replace the magnetic perturbation with its expectation (smoothed at the relevant scale) in the higher order terms only. This is not fully justified, however the magnetic pressure is always positive, and there are large-scale modes that look locally homogeneous, so this prescription aims to include the main qualitative effect of the pressure enhancement due to the large-scale magnetic field being adiabatically compressed. The corresponding effect from large-scale densities compressing the small-scale field has random sign, and hence is expected to have zero mean. In Fourier space this leaves

$$\Delta_B = \Delta_{B,0} + \frac{4}{3}\langle\Delta_{B,0}\rangle_k\Delta_b, \tag{A12}$$

$$\Pi_B^{ij} = \Pi_{B,0}^{ij}, \tag{A13}$$

where the expectation is evaluated using only modes larger than the scale of interest. The equation for Π_B has only the lowest order term as $\langle\Pi_{B,0}\rangle_k = 0$. As a caveat we note that this averaging procedure it unlikely to be valid if the objective is to study nonlinear collapse at density peaks: the large-scale background field changes from place to place, and the density of collapsed objects is expected to be correspondingly modulated. For calculating the power spectrum it may however be a reasonable approximation, and our later results are in fact most constrained by the power spectrum.

Inserting (A12) into (A11) gives

$$\dot{\theta}_b = -\mathcal{H}\theta_b + k^2c_{s,b}^2\Delta_b + k^2\Psi + R\tau_c^{-1}(\theta_\gamma - \theta_b) + \frac{1}{2}k^2R\left(\frac{1}{2}\Delta_{B,0} - \frac{1}{3}\Pi_{B,0}^{(0)}\right) + \frac{2}{9}k^2v_A^2\Delta_b, \tag{A14}$$

where we have defined the Alfvén velocity v_A as

$$v_A^2 = \frac{1}{4\pi\rho a^4}\langle\hat{B}^2\rangle_k = \frac{3}{2}R\langle\Delta_{B,0}\rangle_k, \tag{A15}$$

where ρ is the density of the conducting fluid. The last equality comes from the fact that during matter domination $\rho = \rho_b$. This is the standard evolution Eq. (A11) with a new effective sound speed $c_s^2 \to c_s^2 + \frac{2}{9}v_A^2$. This agrees with other approximate treatments of the magnetic Jeans effect in the literature up to the factor of $\frac{2}{9}$ [36,38,40], which is different but of the same order. This discrepancy has little effect on the magnetic Jeans scale, changing it by at most a factor of 2.

APPENDIX B: SUNYAEV—ZEL'DOVICH EFFECT

In order to compare to the recent data from the South Pole Telescope [53], we need to be able to calculate SZ angular power spectra from linear matter power spectra. We use the halo method of Komatsu and Seljak [54], and largely follow details of the calculation in [53]. We give an outline of this below.

The angular power spectrum is given by

$$C_l = g_\nu^2 \int dz \frac{dV_c}{dz} \int dM \frac{dn(M,z)}{dM} |y_l(M,z)^2|. \tag{B1}$$

In the above V_c is the comoving volume out to redshift z, and g_ν is the spectral function given by

$$g_\nu = \frac{x}{\tanh(x/2)} - 4, \tag{B2}$$

where $x = h\nu/k_B T_{\rm CMB}$. The halo mass function $\frac{dn}{dM}$ is comoving number density of virialized halos at mass M. Finally y_l is the Fourier transform of the projected Compton y profile

$$y_l(M,z) = \frac{4\pi r_s}{l_s^2} \int_0^\infty y_{3D}(x) \mathrm{sinc}(lx/l_s) x^2 dx, \tag{B3}$$

where r_s is the scale radius of the profile, $l_s = d_a/r_s$ is its angular projection (d_a is the angular diameter distance to redshift z) and y_{3D} is the three-dimensional Compton profile in terms of $x = r/r_s$. The profile y_{3D} is determined by the model chosen for the baryon density and temperature profile of the halo. Following the details of [54], we fix its form with four assumptions: the dark matter density profile is Navarro-Frenk-White (NFW) [59]; hydrostatic equilibrium between the gas pressure and the halo self-gravity; baryon density traces the dark matter density in the outer halo; and the gas has a polytropic equation of state $P_b \propto \rho_b^\gamma$. The results of this are given below, for details see [54].

Using an NFW dark matter profile, the scale radius above r_s is the usual NFW definition, $r_s = r_{\rm vir}/c$ where c is the concentration, and $r_{\rm vir}$ is the virial radius given by

$$r_{\rm vir} = \left(\frac{3}{4\pi} \frac{M}{\Delta_c \rho_{\rm cr}}\right)^{1/3}, \tag{B4}$$

where the virialization parameter Δ_c can be calculated from the spherical collapse of a top hat perturbation. A fitting formula for Δ_c is calculated in [60]

$$\Delta_c(z) = 18\pi^2 - 82\Omega_\Lambda(z) + 39\Omega_\Lambda(z)^2 \tag{B5}$$

which is accurate in the range $\Omega_\Lambda < 0.9$.

The concentration parameter c which defines the scale radius of the profile can be fitted from simulations. We use the relation of [61] which takes the form

$$c(M,z) \approx \frac{7.85}{(1+z)^{0.71}} \left(\frac{M}{M_*}\right)^{-0.081}, \tag{B6}$$

where the pivot mass is fixed to be $M_* = 2 \times 10^{12} h^{-1} M_\odot$.

The profile y_{3D} is given by

$$y_{3D}(x) = 1.14 \times 10^{-4}\ \mathrm{Mpc}^{-1} \left[\frac{\rho_b(0)}{10^{14} M_\odot \mathrm{Mpc}^{-3}}\right] \times \left[\frac{k_B T_b(0)}{8\ \mathrm{keV}}\right] y(x). \tag{B7}$$

The dimensionless function $y(x)$ gives the profile shape

$$y(x) = [1 - B[1 - x^{-1} \ln(1+x)]]^{\gamma/(\gamma-1)}. \tag{B8}$$

B is a constant given by

$$B \equiv 3\eta^{-1} \frac{\gamma - 1}{\gamma} \left[\frac{1}{c} \ln(1+c) - \frac{1}{1+c}\right]^{-1}. \tag{B9}$$

Fitting functions for η and γ are derived in [54]. They are valid for the range $1 < c < 25$,

$$\gamma = 1.137 + 0.0894 \ln(c/5) - 3.68 \times 10^{-3}(c - 5), \tag{B10}$$

$$\eta = 2.235 + 0.202(c - 5) - 1.16 \times 10^{-3}(c - 5)^2. \tag{B11}$$

The central gas density $\rho_b(0)$ is

$$\rho_b(0) = 7.96 \times 10^{12} M_\odot \mathrm{Mpc}^{-3} \left(\frac{M}{10^{14} M_\odot}\right)\left(\frac{r_{\rm vir}}{\rm Mpc}\right)^3 \times \left(\frac{\Omega_b}{\Omega_m}\right) \frac{y(x)^{-1/\gamma}}{(1+c)^2} \left[\frac{1}{c} \ln(1+c) - \frac{1}{1+c}\right]^{-1}, \tag{B12}$$

and the central temperature $T_b(0)$ is

$$T_b(0) = 0.880\ \mathrm{keV}\, \eta \left(\frac{M}{10^{14} M_\odot}\right)\left(\frac{r_{\rm vir}}{\rm Mpc}\right)^{-1}. \tag{B13}$$

The final ingredient needed to calculate the SZ power spectrum is the mass function. In common with [53,54] we use the Jenkins mass function [62] calculated from N-body simulations. As with the Press-Schechter prescription the key quantity is the smoothed variance $\sigma(R)$ defined by

$$\sigma^2(R; z) = \int d\ln k \tilde{W}_R^2(k) \mathcal{P}(k; z). \tag{B14}$$

In our work we choose a window function $\tilde{W}_R(k)$ that is a spherical top hat in real space. The mass enclosed in this comoving scale is simply $M = 4\pi\rho_{m,0} R^3/3$, and this defines an obvious mapping between a mass smoothed $\sigma(M)$ and $\sigma(R)$. In terms of $\sigma(M)$ the mass function of [62] is

$$\frac{M^2}{\rho_{m,0}} \frac{dn(M;z)}{dM} = 0.301 \left|\frac{d\ln\sigma}{d\ln M}\right| \exp(-|0.64 - \ln\sigma|). \tag{B15}$$

[1] L. M. Widrow, Rev. Mod. Phys. **74**, 775 (2002).
[2] R. M. Kulsrud and E. G. Zweibel, Rep. Prog. Phys. **71**, 046901 (2008).
[3] C. J. Hogan, Phys. Rev. Lett. **51**, 1488 (1983).
[4] R. Durrer and C. Caprini, J. Cosmol. Astropart. Phys. 11 (2003) 010.
[5] V. Demozzi, V. Mukhanov, and H. Rubinstein, J. Cosmol. Astropart. Phys. 8 (2009) 025.
[6] M. L. Bernet, F. Miniati, S. J. Lilly, P. P. Kronberg, and M. Dessauges-Zavadsky, Nature (London) **454**, 302 (2008).
[7] K. Subramanian and J. D. Barrow, Phys. Rev. Lett. **81**, 3575 (1998).
[8] A. Mack, T. Kahniashvili, and A. Kosowsky, Phys. Rev. D **65**, 123004 (2002).
[9] T. Kahniashvili and B. Ratra, Phys. Rev. D **71**, 103006 (2005).
[10] R. Gopal and S. K. Sethi, Phys. Rev. D **72**, 103003 (2005).
[11] T. Kahniashvili, Y. Maravin, and A. Kosowsky, Phys. Rev. D **80**, 023009 (2009).
[12] M. Giovannini and K. E. Kunze, Phys. Rev. D **78**, 023010 (2008).
[13] F. Finelli, F. Paci, and D. Paoletti, Phys. Rev. D **78**, 023510 (2008).
[14] D. Paoletti, F. Finelli, and F. Paci, Mon. Not. R. Astron. Soc. **396**, 523 (2009).
[15] D. G. Yamazaki, K. Ichiki, T. Kajino, and G. J. Mathews, Phys. Rev. D **77**, 043005 (2008).
[16] J. R. Shaw and A. Lewis, Phys. Rev. D **81**, 043517 (2010).
[17] D. G. Yamazaki, K. Ichiki, K. Umezu, and H. Hanayama, Phys. Rev. D **74**, 123518 (2006).
[18] S. K. Sethi, B. B. Nath, and K. Subramanian, arXiv:0804.3473.
[19] D. G. Yamazaki, K. Ichiki, T. Kajino, and G. J. Mathews, Phys. Rev. D **78**, 123001 (2008).
[20] H. Tashiro and N. Sugiyama, arXiv:0908.0113.
[21] D. G. Yamazaki, K. Ichiki, T. Kajino, and G. J. Mathews, Phys. Rev. D **81**, 103519 (2010).
[22] K. E. Kunze, Phys. Rev. D **83**, 023006 (2011).
[23] J. J. Matese and R. F. O'Connell, Astrophys. J. **160**, 451 (1970).
[24] D. Grasso and H. R. Rubinstein, Phys. Lett. B **379**, 73 (1996).
[25] C. Caprini and R. Durrer, Phys. Rev. D **65**, 023517 (2001).
[26] K. Dolag, M. Bartelmann, and H. Lesch, Astron. Astrophys. **348**, 351 (1999).
[27] R. Banerjee and K. Jedamzik, Phys. Rev. D **70**, 123003 (2004).
[28] D. G. Yamazaki, K. Ichiki, T. Kajino, and G. J. Mathews, Astrophys. J. **646**, 719 (2006).
[29] D. G. Yamazaki, K. Ichiki, T. Kajino, and G. J. Mathews, Phys. Rev. D **81**, 023008 (2010).
[30] D. Paoletti and F. Finelli, Phys. Rev. D **83**, 123533 (2011).
[31] I. Brown and R. Crittenden, Phys. Rev. D **72**, 063002 (2005).
[32] T. R. Seshadri and K. Subramanian, Phys. Rev. Lett. **103**, 081303 (2009).
[33] C. Caprini, F. Finelli, D. Paoletti, and A. Riotto, J. Cosmol. Astropart. Phys. 06 (2009) 021.
[34] R. Durrer, Fundam. Cosmic. Phys. **15**, 209 (1994).
[35] R. Durrer and N. Straumann Helv. Phys. Acta **61**, 1027 (1998).
[36] K. Subramanian and J. D. Barrow, Phys. Rev. D **58**, 083502 (1998).
[37] K. Jedamzik, V. Katalinić, and A. V. Olinto, Phys. Rev. D **57**, 3264 (1998).
[38] E. Kim, A. V. Olinto, and R. Rosner, Astrophys. J. **468**, 28 (1996).
[39] J. D. Barrow, R. Maartens, and C. G. Tsagas, Phys. Rep. **449**, 131 (2007).
[40] J. Adams, U. H. Danielsson, D. Grasso, and H. Rubinstein, Phys. Lett. B **388**, 253 (1996).
[41] S. K. Sethi and K. Subramanian, Mon. Not. R. Astron. Soc. **356**, 778 (2005).
[42] A. Lewis, A. Challinor, and A. Lasenby, Astrophys. J. **538**, 473 (2000).
[43] A. Lewis and S. Bridle, Phys. Rev. D **66**, 103511 (2002).
[44] N. Jarosik, C. L. Bennett, J. Dunkley, B. Gold, M. R. Greason, M. Halpern, R. S. Hill, G. Hinshaw, A. Kogut, E. Komatsu *et al.*, Astrophys. J., Suppl. Ser. **192**, 014 (2011).
[45] M. L. Brown, P. Ade, J. Bock, M. Bowden, G. Cahill, P. G. Castro, S. Church, T. Culverhouse, R. B. Friedman, K. Ganga *et al.*, Astrophys. J. **705**, 978 (2009).
[46] C. L. Reichardt, P. A. R. Ade, J. J. Bock, J. R. Bond, J. A. Brevik, C. R. Contaldi, M. D. Daub, J. T. Dempsey, J. H. Goldstein, W. L. Holzapfel *et al.*, Astrophys. J. **694**, 1200 (2009).
[47] W. L. Freedman *et al.*, Astrophys. J. **553**, 47 (2001).
[48] M. Kowalski *et al.*, Astrophys. J. **686**, 749 (2008).
[49] W. J. Percival *et al.*, Mon. Not. R. Astron. Soc. **401**, 2148 (2010).
[50] S. Cole *et al.* (The 2dFGRS), Mon. Not. R. Astron. Soc. **362**, 505 (2005).
[51] M. Tegmark *et al.*, Phys. Rev. D **74**, 123507 (2006).
[52] B. A. Reid *et al.*, Mon. Not. R. Astron. Soc. **404**, L60 (2010).
[53] M. Lueker, C. L. Reichardt, K. K. Schaffer, O. Zahn, P. A. R. Ade, K. A. Aird, B. A. Benson, L. E. Bleem, J. E. Carlstrom, C. L. Chang *et al.*, Astrophys. J. **719**, 1045 (2010).
[54] E. Komatsu and U. Seljak, Mon. Not. R. Astron. Soc. **336**, 1256 (2002).
[55] P. Zhang and R. K. Sheth, Astrophys. J. **671**, 14 (2007).
[56] P. McDonald, U. Seljak, R. Cen, D. Shih, D. H. Weinberg, S. Burles, D. P. Schneider, D. J. Schlegel, N. A. Bahcall, J. W. Briggs *et al.*, Astrophys. J. **635**, 761 (2005).
[57] M. Maggiore, arXiv:gr-qc/0008027.
[58] C. Caprini and R. Durrer, Phys. Rev. D **72**, 088301 (2005).
[59] J. F. Navarro, C. S. Frenk, and S. D. M. White, Astrophys. J. **490**, 493 (1997).
[60] G. L. Bryan and M. L. Norman, Astrophys. J. **495**, 80 (1998).
[61] A. R. Duffy, J. Schaye, S. T. Kay, and C. Dalla Vecchia, Mon. Not. R. Astron. Soc. **390**, L64 (2008).
[62] A. Jenkins, C. S. Frenk, S. D. M. White, J. M. Colberg, S. Cole, A. E. Evrard, H. M. P. Couchman, and N. Yoshida, Mon. Not. R. Astron. Soc. **321**, 372 (2001).